

SiameseNorm: Breaking the Barrier to Reconciling Pre/Post-Norm

Tianyu Li^{*1,2}, Dongchen Han^{*1}, Zixuan Cao³, Haofeng Huang³, Mengyu Zhou^{†2}, Ming Chen², Erchao Zhao², Xiaoxi Jiang², Guanjun Jiang² and Gao Huang^{†1}

¹Leap Lab, Tsinghua University, ²Qwen Large Model Application Team, Alibaba, ³Institute for Interdisciplinary Information Sciences, Tsinghua University

* Equal Contribution. [†]Corresponding author(s).

Modern Transformers predominantly adopt the Pre-Norm paradigm for its optimization stability, foregoing the superior potential of the unstable Post-Norm architecture. Prior attempts to combine their strengths typically lead to a stability-performance trade-off. We attribute this phenomenon to a structural incompatibility within a *single-stream* design: Any application of the Post-Norm operation inevitably obstructs the clean identity gradient preserved by Pre-Norm. To fundamentally reconcile these paradigms, we propose SiameseNorm, a *two-stream* architecture that couples Pre-Norm-like and Post-Norm-like streams with shared parameters. This design decouples the optimization dynamics of the two streams, retaining the distinct characteristics of both Pre-Norm and Post-Norm by enabling all residual blocks to receive combined gradients inherited from both paradigms, where one stream secures stability while the other enhances expressivity. Extensive pre-training experiments on 1.3B-parameter models demonstrate that SiameseNorm exhibits exceptional optimization robustness and consistently outperforms strong baselines. Code is available at github.com/Qwen-Applications/SiameseNorm.

1. Introduction

Layer Normalization (Ba et al., 2016) (LN) and its variants, such as RMSNorm (Zhang & Sennrich, 2019), serve as essential components in modern deep learning architectures, enabling stable optimization of deep networks, particularly Transformers (Vaswani et al., 2017). A key architectural decision when employing LN is where to apply it in each residual update, as it fundamentally shapes the gradient flow, the activation scaling, and the effective depth. The two primary paradigms are Post-Norm (Vaswani et al., 2017) and Pre-Norm (Wang et al., 2019): Pre-Norm applies LN to the input of the residual branch, whereas Post-Norm applies LN after the residual addition. Currently, large-scale models (Brown et al., 2020; Touvron et al., 2023b; Liu et al., 2024; Yang et al., 2025; Dosovitskiy, 2020) predominantly adopt the Pre-Norm architecture for its superior training stability. However, this stability comes at a cost: empirical studies show that pruning a significant fraction of deep layers in Pre-Norm models often only results in negligible performance drops (Gromov et al., 2025; Sun et al., 2025), suggesting restricted effective depth and representational capacity under the Pre-Norm design.

In contrast, Post-Norm is widely recognized for its higher performance upper bound compared to Pre-Norm thanks to its strong representation dynamics (Vaswani et al., 2017; Wang et al., 2024). However, as models scale up, ensuring stable training of Post-Norm Transformers becomes increasingly challenging. Prior analyses (Wang et al., 2024) reveal that this instability stems from the tendency of gradients

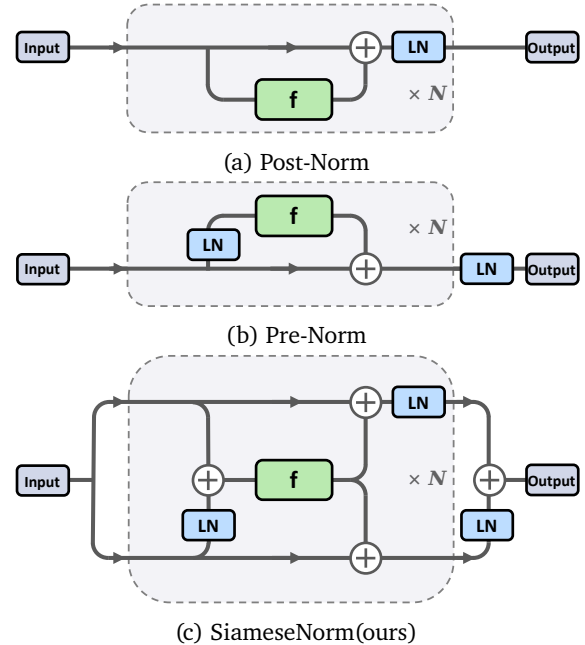


Figure 1 | Architectural comparison of Post-Norm, Pre-Norm and SiameseNorm. In SiameseNorm, the input is duplicated into parallel streams sharing identical residual updates, where distinct LN positioning differentiates the hidden states across layers.

to vanish or explode, which is often catastrophic in the context of large-scale pre-training. Empirical evidence (Liu et al., 2020; Xiong et al., 2020) demonstrates that due to

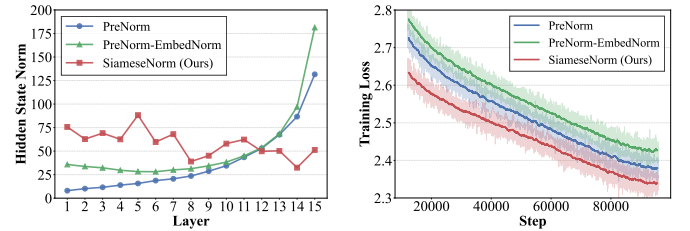
this inherent instability, Post-Norm requires conservative training settings to avoid divergence, while Pre-Norm often attains better performance by employing more aggressive hyperparameters within the same training budget. This optimization gap implies that Post-Norm frequently fails to fully realize its theoretical performance potential.

Extensive efforts in the community have been devoted to designing advanced normalization schemes with improved expressiveness, trainability, and scalability. A natural strategy is to combine Pre-Norm and Post-Norm to leverage the complementary strengths of both. In practice, however, such hybrid designs (Zhuo et al., 2025; Li et al., 2025) often lack training robustness outside specific settings, inheriting the instability of Post-Norm. We attribute this to an intrinsic tension between the two paradigms: Pre-Norm stabilizes deep networks by preserving an identity path where the signal magnitude would increase naturally across layers, whereas Post-Norm does the exact opposite by strictly regulating the signal after each residual addition. Therefore, attempting to enforce both mechanisms within a *single-stream* inevitably leads to a compromise where neither objective is fully met.

In this paper, we propose **SiameseNorm**, an elegant *two-stream* residual architecture that unifies Pre-Norm and Post-Norm behaviors within each layer. The core idea is to maintain two residual streams with shared parameters: one stream preserves an unnormalized hidden representation to retain the clean identity gradient characteristic of Pre-Norm, while the other maintains a regularized hidden state via normalization to recover the depth-wise representation dynamics of Post-Norm. By decoupling identity gradient from controlled representation scale, and fusing them prior to each computation module, SiameseNorm achieves the advantages of the two paradigms with negligible computational overhead. We validate this approach through extensive pre-training of 1.3B parameter models, demonstrating that SiameseNorm effectively mitigates the optimization instability of Post-Norm and supports aggressive learning rates. Our results show that SiameseNorm substantially outperforms strong baselines including Pre-Norm, Post-Norm, Hybrid-Norm variants, and Hyper-Connections, resolving the long-standing stability-efficiency dilemma in large-scale model training. Notably, on basic arithmetic tasks, SiameseNorm boosts accuracy from 28.1 (Pre-Norm) to 39.6. This 40.9% relative gain over Pre-Norm provides empirical evidence that it successfully restores the network’s effective depth, crucial for sequential reasoning capabilities.

2. Theoretical Motivation

We now formalize the behavior of Pre-Norm and Post-Norm residual blocks and analyze their gradient dynamics to high-



(a) Final batch-averaged layer-wise hidden state magnitudes.

(b) Training loss curves.

Figure 2 | Comparison of Pre-Norm, PreNorm-EmbedNorm, and our SiameseNorm using 1.3B models trained on 100B tokens with learning rate of 1×10^{-3} .

light their respective optimization challenges, revealing the inherent structural incompatibility of existing paradigms.

2.1. Preliminaries

Notation Consider a generic Transformer layer with input $X_i \in \mathbb{R}^d$ and output $X_{i+1} \in \mathbb{R}^d$, where $i = 0, \dots, N - 1$, and N denotes the total number of layers. For any hidden state X_i , we define its **magnitude** as the ℓ_2 -norm, denoted by $\|X_i\|_2$. Throughout our analysis, we track the evolution of this magnitude across successive layers to characterize the signal scaling behavior of different normalization strategies.

Let $F_i(\cdot)$ denote the residual transformation (e.g., Attention or MLP) and θ_i denote its parameters, so that $\nabla_{\theta_i} \mathcal{L}$ represents the parameter gradients. We use LN to denote generic normalization (e.g., LayerNorm or RMSNorm), noting that the specific variant does not alter the qualitative gradient dynamics discussed herein. Finally, let $\mathbf{J}_F \triangleq \frac{\partial F(X)}{\partial X}$ denote the Jacobian of a function F .

Taxonomy of Normalization Paradigms To facilitate our analysis, we categorize existing architectures based on the evolution of their hidden state magnitudes.

(i) **Pre-Norm Paradigm:** In this paradigm, LN is only placed in the residual branch, allowing the hidden state magnitude to grow implicitly. The forward pass of the standard Pre-Norm (Figure 1b) is defined as:

$$X_{i+1} = X_i + F_i(\text{LN}_i(X_i)) \quad (1)$$

This family includes standard Pre-Norm and variants like Hyper-Connections (Zhu et al., 2025a; Xie et al., 2025), where the residual updates are accumulated into an ever-expanding main path.

(ii) **Post-Norm Paradigm:** Architectures in this family explicitly rescale the hidden representation to enforce a fixed magnitude periodically. The formulation of the standard

Post-Norm (Figure 1a) is as follows:

$$X_{i+1} = \text{LN}_i(X_i + F_i(X_i)) \quad (2)$$

This family includes the standard Post-Norm and variants such as HybridNorm (Zhuo et al., 2025), which apply normalization to the main path only after Attention blocks.

2.2. Evaluation of Existing Paradigms

Pre-Norm The loss gradient \mathcal{L} with respect to θ_i under the Pre-Norm defined in Equation (1) is given by:

$$\nabla_{\theta_i} \mathcal{L} = \frac{\partial \mathcal{L}}{\partial X_N} \left(\prod_{j=N-1}^{i+1} \frac{\partial X_{j+1}}{\partial X_j} \right) \frac{\partial X_{i+1}}{\partial \theta_i} \quad (3)$$

$$= \frac{\partial \mathcal{L}}{\partial X_N} \left[\prod_{j=N-1}^{i+1} \left(\mathbf{I} + \frac{\partial F_j(\text{LN}_j(X_j))}{\partial X_j} \right) \right] \frac{\partial X_{i+1}}{\partial \theta_i} \quad (4)$$

$$= \frac{\partial \mathcal{L}}{\partial X_N} \left[\prod_{j=N-1}^{i+1} \left(\mathbf{I} + \mathbf{J}_{F_j} \mathbf{J}_{\text{LN}_j} \right) \right] \frac{\partial X_{i+1}}{\partial \theta_i}, \quad (5)$$

where the product denotes an ordered composition of Jacobians from layer $N-1$ down to $i+1$. Notably, the term \mathbf{I} corresponds to the skip connection, which preserves an explicit identity gradient path. This allows gradients to flow through the network without explicit attenuation, facilitating the training of large scale models. However, it implicitly allows the representation magnitudes to grow unbounded. As noted previously, Pre-Norm exhibits insufficient effective depth, an issue that likely stems from a structural mismatch: As shown in Figure 2a, the main path accumulates residual updates without re-normalization, causing hidden state magnitudes to grow with depth (Kim et al., 2025). Consequently, deeper blocks encounter a scaling imbalance: they must influence an increasingly high-magnitude main path while being restricted to normalized, fixed-scale inputs. This growing disparity effectively dilutes the relative contribution of deeper layers, thereby limiting the effective depth of the model.

Motivated by this intuition, we conducted an exploratory experiment to assess the sensitivity of Pre-Norm to initial magnitude scaling. We introduced a parameter-free RMSNorm applied after the embedding layer. This variant, denoted PreNorm-EmbedNorm in Figure 2a, explicitly rescales the initial hidden state X_0 , forcing its magnitude to increase to \sqrt{d} . In our setup, this intervention amplifies the initial magnitude from approximately 2 to 45. Although this modification successfully suppressed the magnitude growth in the early layers, yielding a nearly flat magnitude profile, it resulted in severe performance degradation, specifically a perplexity degradation of 0.4. This negative result underscores the intrinsic difficulty of regulating the representation magnitude within Pre-Norm frameworks.

Post-Norm As defined in Equation (2), Post-Norm integrates the normalization layer into the main branch, effectively resetting the second-order statistics of the residual sum at each layer, keeping the scale of representations invariant across depth. However, backpropagation requires multiplying the gradients by the LN Jacobian at each layer:

$$\nabla_{\theta_i} \mathcal{L} = \frac{\partial \mathcal{L}}{\partial X_N} \left(\prod_{j=N-1}^{i+1} \frac{\partial X_{j+1}}{\partial X_j} \right) \frac{\partial X_{i+1}}{\partial \theta_i} \quad (6)$$

$$= \frac{\partial \mathcal{L}}{\partial X_N} \left[\prod_{j=N-1}^{i+1} \mathbf{J}_{\text{LN}_j} (\mathbf{I} + \mathbf{J}_{F_j}) \right] \frac{\partial X_{i+1}}{\partial \theta_i} \quad (7)$$

Even if $\mathbf{I} + \mathbf{J}_{F_j}$ is well-conditioned, repeated application of \mathbf{J}_{LN} causes multiplicative instability. Since the spectral norm of \mathbf{J}_{LN} is sensitive to the signal, this compounding effect can cause gradients to vanish or explode as the depth N increases. This mechanism explains the severe optimization instability observed in deep Post-Norm Transformers.

2.3. Structural Incompatibility

Although prior approaches (Li et al., 2025; Zhuo et al., 2025) attempt to reconcile Pre-Norm and Post-Norm, our empirical observations (Table 1) suggest that they generally fail to escape the trade-off between stability and performance. We argue that this is not merely an implementation issue, but a fundamental structural incompatibility rooted in the geometry of the residual path. The core conflict lies in the treatment of the main signal path:

The Dilution Problem (Pre-Norm) By maintaining a clean identity path, Pre-Norm ensures stable gradient propagation. However, this comes at the cost of unbounded magnitude growth. As illustrated in Figure 2a, while the input to the residual block is structurally constrained to a constant level, the hidden state magnitude exhibits near-exponential growth. This growing disparity creates a severe optimization burden: to maintain a meaningful relative contribution against the massive main path, deeper layers are compelled to learn increasingly large output magnitudes. The difficulty of learning such extreme scalings typically results in signal dilution, severely limiting the model’s effective depth.

The Distortion Problem (Post-Norm) By enforcing explicit normalization, Post-Norm maintains unit-scale hidden state magnitudes across layers. However, this imposes repeated scale contractions on the main path. Since residual addition inherently expands the signal, the normalization layer must aggressively shrink the representation back to a fixed scale at each step. This process inherently

destroys scale information and distorts gradient geometry, leading to compounding instability.

Existing hybrid methods typically oscillate between these two extremes by alternating blocks without resolving the underlying algebraic conflict: it is mathematically impossible to preserve the strict identity path essential for gradient propagation while simultaneously enforcing the bounded constraints required for representation efficiency *within a shared main path*. This necessitates structural decoupling rather than a straightforward combination.

3. SiameseNorm

Architecture and Formulation Now, we introduce our proposed architecture, SiameseNorm. As illustrated in Figure 1c, SiameseNorm resolves the tension between Pre-Norm and Post-Norm by introducing two coupled streams per layer: One preserves an identity gradient path and the other maintains bounded representations. Crucially, both streams share the same residual block F_i , ensuring that the parameter count remains essentially unchanged. Let X_i and Y_i denote the states of the bounded (Post-Norm-like) and unbounded (Pre-Norm-like) streams at layer i , respectively. We initialize both streams with the input embeddings:

$$X_0 = Y_0 = \text{input}.$$

At each layer i , we perform the following updates:

$$\begin{aligned} Y'_i &= \text{LN}_i^Y(Y_i), \\ O_i &= F_i(X_i + Y'_i), \\ X_{i+1} &= \text{LN}_i^X(X_i + O_i), \\ Y_{i+1} &= Y_i + O_i. \end{aligned}$$

Specifically, F_i operates on the aggregation of the bounded state X_i and the normalized unbounded state Y'_i . At layer N , the two streams are fused to produce the final representation:

$$X_{\text{output}} = X_N + \text{LN}_{\text{final}}(Y_N).$$

Intuitively, the Y -stream follows a Pre-Norm residual topology: it accumulates updates O_i onto an unnormalized stream Y_i , preserving the identity gradient path. Conversely, the X -stream mirrors a Post-Norm topology: it applies normalization LN_i^X after residual addition, enforcing explicit bounds on the representation scale.

Generalization Capabilities A key property of SiameseNorm is that it strictly generalizes Pre-Norm, Post-Norm, and hybrid schemes. Specifically: (i) Zeroing the parameters of LN_i^X eliminates the bounded stream, recovering the Pre-Norm topology; (ii) Zeroing LN_i^Y isolates the bounded stream, reducing the architecture to Post-Norm; (iii) Intermediate configurations encompass hybrid designs such as Mix-LN (Li et al., 2025). Thus, our design subsumes these

paradigms as special cases, making the best performance among these special cases a lower bound of the achievable performance of SiameseNorm.

Gradient Analysis Let $S_i = [X_i, Y_i]^\top$ be the concatenated state of the two streams. Examine the loss gradient \mathcal{L} with respect to the residual transformation parameters θ_i :

$$\begin{aligned} \nabla_{\theta_i} \mathcal{L} &= \frac{\partial \mathcal{L}}{\partial S_N} \left(\prod_{j=N-1}^{i+1} \frac{\partial S_{j+1}}{\partial S_j} \right) \frac{\partial S_{i+1}}{\partial O_i} \frac{\partial O_i}{\partial \theta_i} \\ &= \frac{\partial \mathcal{L}}{\partial S_N} \left(\prod_{j=N-1}^{i+1} \frac{\partial S_{j+1}}{\partial S_j} \right) \begin{bmatrix} \mathbf{J}_{\text{LN}_i^X} & \mathbf{I} \\ \mathbf{I} & \mathbf{I} + \mathbf{J}_{F_i} \mathbf{J}_{\text{LN}_i^Y} \end{bmatrix} \frac{\partial O_i}{\partial \theta_i} \end{aligned}$$

The block Jacobian transition matrix is given by:

$$\frac{\partial S_{j+1}}{\partial S_j} = \begin{bmatrix} \mathbf{J}_{\text{LN}_j^X} (\mathbf{I} + \mathbf{J}_{F_j}) & \mathbf{J}_{\text{LN}_j^X} \mathbf{J}_{F_j} \mathbf{J}_{\text{LN}_j^Y} \\ \mathbf{J}_{F_j} & \mathbf{I} + \mathbf{J}_{F_j} \mathbf{J}_{\text{LN}_j^Y} \end{bmatrix} \quad (8)$$

The diagonal blocks of this transition matrix reveal a structural correspondence to the standard LN paradigms. The bottom-right block, $\mathbf{I} + \mathbf{J}_{F_j} \mathbf{J}_{\text{LN}_j^Y}$, structurally replicates the gradient dynamics of Pre-Norm, as derived in Equation (5). The presence of the explicit identity term \mathbf{I} guarantees a robust gradient highway for all residual outputs, effectively preventing vanishing gradients. On the other hand, the top-left block, $\mathbf{J}_{\text{LN}_j^X} (\mathbf{I} + \mathbf{J}_{F_j})$, aligns with the Post-Norm formulation described in Equation (7). Here, the gradient flow is modulated by the normalization Jacobian \mathbf{J}_{LN_j} , which strictly enforces bounded representation scales on the X -stream. Consequently, SiameseNorm essentially executes both Pre-Norm and Post-Norm optimization mechanisms in parallel, inheriting the stability of the former and the bounded representation capability of the latter within a unified architecture.

Computational Overhead Compared to a standard Pre-Norm Transformer, SiameseNorm introduces only auxiliary LN operations. Since the parameters and computation for normalization are minimal compared to the heavy Attention and MLP blocks, the resulting overhead is negligible.

4. Experiments

4.1. Experimental Setup

Architecture and Training Setup We conduct controlled comparisons based on the OLMo (Groeneveld et al., 2024) architecture trained from scratch on FineWeb-Edu (Penedo et al., 2024). Given the sensitivity of training stability and final performance to the learning rate, we evaluate three learning rates (4×10^{-4} , 10^{-3} , and 2×10^{-3}) trained for 100B tokens. Additionally, we extend the aggressive

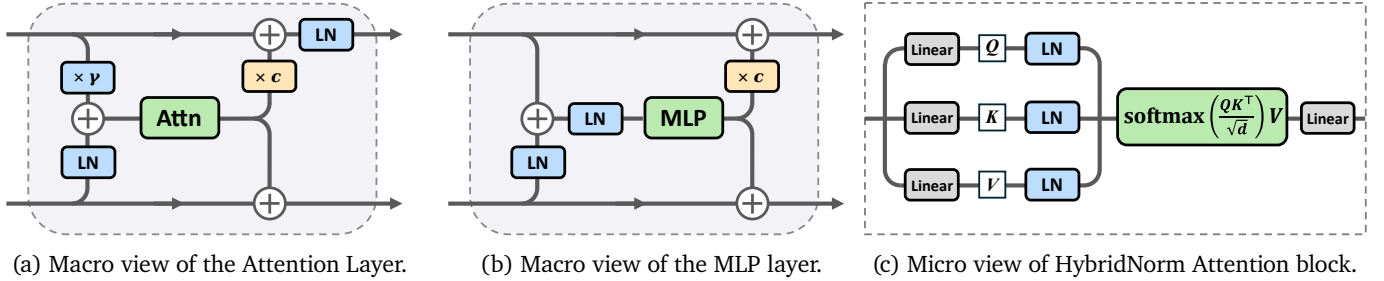


Figure 3 | Practical SiameseNorm design, coupling HybridNorm (Zhuo et al., 2025) and Pre-Norm with HybridNorm Attention blocks.

2×10^{-3} setting to 350B tokens to verify long-term stability. The total computational cost for all experimental results is equivalent to over 50,000 A100 hours. Detailed experimental setup is provided in Section A.2.

Evaluation Protocol We evaluate our models on a diverse suite of benchmarks covering commonsense reasoning (ARC (Clark et al., 2018), HellaSwag (Zellers et al., 2019), PIQA (Bisk et al., 2020), WinoGrande (Sakaguchi et al., 2021)), knowledge-grounded question answering (OpenBookQA (Mihaylov et al., 2018)), and arithmetic reasoning (Arithmetic (Brown et al., 2020)). In addition, we report average perplexity (PPL) in the training data to provide a balanced assessment of reasoning ability, representation quality, and optimization performance.

4.2. Baselines and Implementation Details

We compare SiameseNorm against widely used normalization strategies in Transformer architectures. We include:

- (a) Pre-Norm, applying LN before each residual addition.
- (b) Post-Norm, applying LN after each residual addition.
- (c) DeepNorm (Wang et al., 2024), a Post-Norm variant with depth-dependent residual scaling and initialization.
- (d) ResiDual (Xie et al., 2023), a Post-Norm variant with an additional shortcut from each block to the network output.
- (e) HybridNorm (Zhuo et al., 2025), applying LN after Attention residual and normalizing the input of every block.
- (f) Hyper-Connections-DHC $\times 2$ (Zhu et al., 2025a), a dual-branch pre-norm architecture with mixed paths.

We instantiate our approach (Figure 3) by coupling HybridNorm (Zhuo et al., 2025) with Pre-Norm, as HybridNorm represents a highly competitive variant within the Post-Norm family. To compensate for HybridNorm’s omission of LN after MLP blocks, we introduce a learnable vector γ on the HybridNorm stream to the Attention input to learn the mixing intensity. Crucially, unlike previous multi-path methods (Zhu et al., 2025a) relying on Pre-Norm-biased initialization, we initialize γ and all LN scales to 1.0. This

enforces equal initial stream contribution, thereby rigorously testing the intrinsic stability of our method.

In our investigation, we identified two critical mechanisms required for SiameseNorm: **Normalized Input** and **Depthwise Scaling**. We observe that even though the hidden representations from both streams are normalized prior to fusion, it is crucial to apply an additional LN to the aggregated representation before feeding it into the residual block. This step ensures a stable input distribution for subsequent computation, highlighting the vital role of input normalization in Transformer optimization. Furthermore, a scale mismatch arises as network depth increases: the norms in the Pre-Norm stream tend to grow, whereas the HybridNorm stream remains bounded. This creates a dilemma in deep layers where the shared residual update is either too small to effectively update the Pre-Norm stream, or too large to maintain stability in the HybridNorm stream. To rebalance their contributions, we scale the residual update fed into the HybridNorm stream by $1/\sqrt{l+1}$, where l denotes the layer index. Through ablation studies, we demonstrate that both the core SiameseNorm architecture and these two mechanisms are indispensable for effective optimization.

4.3. Main Results

Table 1 summarizes the performance of various normalization architectures across different learning rate regimes. Our empirical findings lead to the following observations:

LR Sensitivity Obscures Architectural Comparison Under conservative learning rates ($\eta = 4 \times 10^{-4}$), all methods converge successfully, and the HybridNorm outperforms Pre-Norm, demonstrating the potential of Post-Norm paradigm. However, as we increase the learning rate to $\eta = 1 \times 10^{-3}$, the inherent instability of Post-Norm architectures becomes increasingly pronounced. Standard Post-Norm and the previously strong HybridNorm exhibit training divergence. While DeepNorm demonstrates superior stability by successfully converging at this rate with an improved PPL of 11.47, it eventually succumbs to instability and diverges at $\eta = 2 \times 10^{-3}$. The Post-Norm variant

Table 1 | Evaluation results on 1.3B parameter models. We report perplexity (PPL) and accuracy on downstream tasks across three learning rate settings (4×10^{-4} , 1×10^{-3} and 2×10^{-3}). Entries marked as *diverge* denote cases where the model failed to converge, and entries marked with * indicate training runs with loss spikes, signifying training instability.

Method	Avg. PPL \downarrow	ARC-E	ARC-C	HS	OBQA	PIQA	WG	Arith.	Avg. Score \uparrow
Setting A: Conservative Learning Rate ($\eta = 4 \times 10^{-4}$), 100B tokens									
Post-Norm	12.61	67.5	34.1	48.0	36.6	70.6	53.6	27.1	48.21
Deep-Norm	12.95	64.9	30.1	46.5	36.4	69.2	55.7	26.3	47.01
ResiDual	12.32	66.8	33.4	49.6	36.8	71.1	54.5	25.8	48.29
Pre-Norm	11.21	70.2	37.5	54.1	36.2	73.3	56.5	27.7	50.79
Hyper-Connections-2×DHC	11.12	70.9	38.8	54.6	39.0	72.6	55.2	26.9	51.14
HybridNorm	10.91	72.3	38.8	56.4	38.4	74.2	57.0	27.6	52.10
SiameseNorm(Ours)	10.57	72.1	36.8	57.8	40.6	72.5	57.6	28.4	52.26
Setting B: High Learning Rate ($\eta = 1 \times 10^{-3}$), 100B tokens									
Post-Norm	diverge	-	-	-	-	-	-	-	-
Deep-Norm	11.47	68.4	35.4	53.7	38.8	72.1	56.2	27.7	50.33
ResiDual	11.22*	70.0	39.5	55.1	41.2	72.8	57.0	27.5	51.87
Pre-Norm	10.84	71.9	37.8	56.4	39.8	73.8	56.7	27.0	51.91
Hyper-Connections-2×DHC	10.73	72.6	39.1	57.7	41.2	73.8	59.9	27.9	53.17
HybridNorm	diverge	-	-	-	-	-	-	-	-
SiameseNorm (Ours)	10.43	72.5	39.8	59.0	41.0	74.0	59.0	29.4	53.53
Setting C: Aggressive Learning Rate ($\eta = 2 \times 10^{-3}$), 100B tokens									
Deep-Norm	diverge	-	-	-	-	-	-	-	-
HybridNorm	diverge	-	-	-	-	-	-	-	-
ResiDual	13.66*	64.4	33.8	45.2	35.4	69.0	53.6	26.2	46.80
Pre-Norm	10.89	71.6	40.8	57.7	41.4	73.7	57.3	28.1	52.94
Hyper-Connections-2×DHC	10.77	73.7	40.1	58.2	40.0	73.8	60.4	30.6	53.83
SiameseNorm (Ours)	10.48	73.5	38.5	59.6	41.4	74.6	62.2	39.6	55.63
Setting D: Aggressive Learning Rate ($\eta = 2 \times 10^{-3}$), 350B tokens									
Pre-Norm	9.67	78.1	42.8	63.5	41.6	76.0	62.0	36.2	57.17
Hyper-Connections-2×DHC	9.57*	76.3	43.1	63.5	42.4	75.3	61.3	33.6	56.50
SiameseNorm (Ours)	9.42	75.6	44.1	64.7	44.6	76.0	62.5	43.4	58.70

ResiDual exhibits better stability than the vanilla version but suffers from frequent loss spikes. In contrast, Pre-Norm maintains training stability, consistently increasing its average downstream score. This stark contrast highlights a fundamental challenge in architectural evaluation: Pre-Norm and Post-Norm variants often operate in distinct optimum learning rate regimes. Since the choice of learning rate does not affect the computational cost per-step, a strictly fair comparison would require an exhaustive grid search for the optimal η for each variant. However, such a search entails prohibitive computational overhead.

Higher Learning Rates Boost Model Performance Consistent with previous observations (Qiu et al., 2025), our empirical results confirm that increasing learning rate, when training stability is preserved, yields systematic per-

formance improvements in both Pre-Norm and Post-Norm paradigms. This benefit is particularly pronounced on downstream tasks, where all methods that converged without loss spikes under the higher learning rate exhibited significant score gains.

Superiority of SiameseNorm Across all learning rate configurations, our proposed SiameseNorm demonstrates exceptional training stability and performance. In particular, it achieves a performance breakthrough reaching a PPL of 10.43 in Setting B. This represents a significant **reduction of 0.3** compared to the strongest baseline, underscoring that our fusion approach not only inherits the optimization benefits of Pre-Norm but also fully leverages the superior expressive capacity of Post-Norm architectures. Furthermore, with a higher learning rate of 2×10^{-3} ,

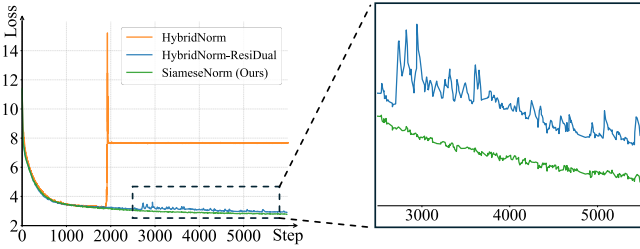


Figure 4 | Training loss curves of HybridNorm (yellow), HybridNorm with ResiDual (blue) and our SiameseNorm (green) without Depth-wise Scaling.

SiameseNorm achieves a substantial accuracy of 39.6% on Arithmetic tasks, far exceeding the random baseline 25% and the range 28% to 31% typical of other methods. This **41% relative improvement** over Pre-Norm further validates the superior capacity of our architecture for sequential reasoning.

4.4. Ablation Study

Efficacy of Siamese Topology To isolate the source of stability, we compare three topologies on HybridNorm: the original single stream, ResiDual (Xie et al., 2023), and our SiameseNorm without Depth-wise scaling. As shown in Figure 4 and Row 1,3 in Table 3, the baselines fail to converge or struggle at high learning rates. In contrast, our Siamese design demonstrates superior robustness, achieving smooth convergence and a PPL of 10.68, outperforming both the diverging HybridNorm and the Pre-Norm baseline (10.84). This confirms that our method effectively synergizes the advantages of both paradigms, yielding a performance gain that exceeds its individual components.

Effect of Depth-wise Scaling Table 3 further demonstrates that Depth-wise Scaling not only elevates the maximum stable learning rate for Post-Norm variants, enabling baseline convergence, but also facilitates effective parameter optimization within our Siamese framework. Consequently, incorporating Depth-wise Scaling into SiameseNorm yields the optimal performance, outperforming the unscaled counterpart by perplexity of 0.25.

Necessity of Normalized Input Although the sub-streams are individually normalized, our ablation (Row 5 vs. Row 6 in Table 3) confirms that normalizing the fused representation is indispensable. This underscores that normalized input is fundamental for Transformer blocks.

Choice of Sub-stream Architectures Preliminary experiments indicate that the performance of SiameseNorm is highly dependent on the efficacy of its individual sub-streams. Table 2 compares coupling Pre-Norm with standard Post-Norm versus the more advanced Hybrid-Norm.

Table 2 | Absolute PPL reduction (vs. Pre-Norm baseline) after coupling Pre-Norm with each variant at different learning rates.

Variant	LR=4 × 10 ⁻⁴	LR=1 × 10 ⁻³	LR=2 × 10 ⁻³
Post-Pre	0.18	0.12	0.17
Hybrid-Pre	0.64	0.41	0.41

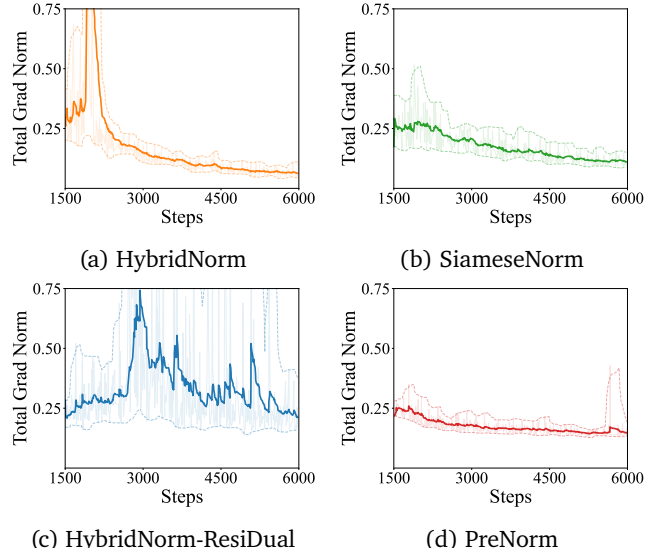


Figure 5 | Gradient norm comparisons

Table 3 | Ablation study of key components in SiameseNorm with learning rate of 10⁻³. The first and last rows denote HybridNorm and our SiameseNorm respectively. Note that normalized input is inherent to HybridNorm and standard Pre/Post-Norm architectures.

Normalized Input	Depth-Scaling	Topology	Avg. PPL ↓
✓	✗	Original	diverge
✓	✓	Original	10.65
✓	✗	ResiDual	11.68*
✓	✗	Siamese	10.68
✗	✓	Siamese	10.51
✓	✓	Siamese	10.43

While the former also provides stability and improves upon its individual components, the overall performance gain is marginal. Conversely, incorporating Hybrid-Norm as a sub-stream yields significantly better results. This confirms that utilizing superior base schemes is essential to unlock the full potential of the SiameseNorm paradigm.

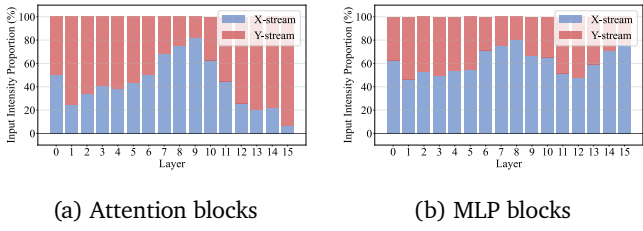


Figure 6 | Comparison of scales ratios for input between the Hybrid-Norm stream (blue) and the Pre-Norm stream (red).

5. Analysis

We now analyze why SiameseNorm works, focusing on gradient statistics and LN parameters.

5.1. Optimization Stability

As shown in Figure 5, to investigate the training stability under high learning rates of 1×10^{-3} , we monitor the gradient norms of different architectures throughout training. As hypothesized, the Post-Norm variant HybridNorm exhibits extreme instability. We observe severe gradient explosions, with gradient norms repeatedly spiking to magnitudes exceeding 100. Such oscillations typically lead to irreversible training divergence. In sharp contrast, SiameseNorm maintains a stable optimization trajectory comparable to Pre-Norm: After the warm-up phase, the gradient norms for both SiameseNorm and Pre-Norm consistently remain below 0.5. This confirms that SiameseNorm successfully inherits the optimization stability of Pre-Norm, effectively mitigating the gradient explosion issues of Post-Norm architectures and enabling more aggressive learning rates.

5.2. Contribution of Each Stream

We further investigate the internal dynamics of SiameseNorm by analyzing the mixing intensity of each stream to the input and conducting a Logit Lens analysis.

Input Intensity Comparison To investigate the internal dynamics of SiameseNorm across layers, we analyze the mixing proportion of each stream to the input. Specifically, we extract the learned scaling parameters of LN from both the Hybrid-Norm stream (X-stream) and the Pre-Norm stream (Y-stream) and normalize them to derive their relative contribution ratios. As illustrated in Figure 6, we observe that for the vast majority of residual blocks, both streams maintain significant proportions. This indicates that SiameseNorm effectively leverages hidden representations from both streams, ensuring that they jointly contribute to the feature extraction process.

Post-Norm Variant Stream Dominance We examine the average learned LN weights at the final fusion layer to quantify each stream’s contribution to the output. The HybridNorm stream converges to a significantly larger weight (1.05) compared to the Pre-Norm stream (0.42). Furthermore, drawing on the intuition of Logit Lens (Geva et al., 2021), we project the final hidden states of each stream directly into the vocabulary space to identify which stream drives model decisions. The HybridNorm stream exhibits clear dominance, matching the final output 42.6% of the time, compared to only 16.2% for the Pre-Norm stream. In divergent predictions, the model aligns with the HybridNorm stream 41.2% of the time, versus just 14.3% for Pre-Norm. This dominance confirms that our approach successfully unlocks the potential of the Post-Norm paradigm.

6. Related Work

Macro-Architectural Designs Foundational residual architectures, such as ResNet (He et al., 2016), Highway Networks (Srivastava et al., 2015) and DenseNet (Huang et al., 2017), demonstrated that explicit shortcut or gating pathways substantially ease optimization and improve depth scalability. A substantial body of work (Wang et al., 2024; Touvron et al., 2021; Bachlechner et al., 2021) improves very-deep optimization through initialization and residual scaling in Transformer. Another line of work modifies the residual topology to alleviate the trade-off between gradient stability and depth utilization: ResiDual (Xie et al., 2023) mitigates Post-Norm instability via per-block shortcuts to the output, while hybrid strategies like MixLN (Li et al., 2025) and HybridNorm (Zhuo et al., 2025) combine Pre-Norm and Post-Norm across layers to balance signal propagation. Recent hidden dimension scaling schemes (Baykal et al., 2023; Zhu et al., 2025a,b; Xie et al., 2025; Han et al., 2025) leverage adaptive widening connections, yet remain confined to the Pre-Norm paradigm. We provide a comprehensive discussion and distinction between our approach and these topology-modifying works in Section A.1.

Micro-Architectural Designs Complementary to macro-topological changes, substantial progress has been made in optimizing the internal sub-layers of the Transformer. In the Feed-Forward Network (FFN), activation functions have evolved from GeLU (Hendrycks, 2016) to GLU variants, particularly SwiGLU (Shazeer, 2020), which have become the default in modern LLMs for their superior performance. Regarding attention mechanisms, Rotary Positional Embeddings (RoPE) (Su et al., 2024) have largely replaced absolute embeddings to enhance length extrapolation, while Grouped-Query Attention (GQA) (Ainslie et al., 2023) is widely adopted to optimize memory bandwidth during inference. Furthermore, to address the quadratic complexity of standard self-attention, sparse attention

mechanisms (Child et al., 2019; Beltagy et al., 2020; Kitaev et al., 2020; Yuan et al., 2025) reduce computation by pruning the attention graph, while linear attention paradigms (Katharopoulos et al., 2020; Choromanski et al., 2020; Gu & Dao, 2023; Han et al., 2023, 2024; Team et al., 2025; Chen et al., 2025) achieve linear scaling with respect to sequence length.

Depth Pathologies in Pre-Norm Transformers While Pre-Norm has become the de facto standard for its optimization robustness (Brown et al., 2020; Touvron et al., 2023a; Dosovitskiy, 2020; Xiong et al., 2020), recent work suggests that very deep Pre-Norm Transformers can exhibit degraded depth utilization (Gromov et al., 2025). A critical limitation of Pre-Norm identified in recent literature is that the unnormalized residual stream can increase in magnitude with depth, creating a scale mismatch between the main path and normalized inputs to residual branches (Sun et al., 2025; Kim et al., 2025).

LayerNorm Variants Layer Normalization (LN) (Ba et al., 2016) is a key component in stabilizing Transformer optimization. Beyond the standard LN, commonly used variants modify the normalization operator itself, such as RMSNorm (Zhang & Sennrich, 2019) and ScaleNorm (Nguyen & Salazar, 2019). Other approaches alter the placement or frequency of normalization, such as Sandwich-Norm (Ding et al., 2021; Kim et al., 2025) and QK-Norm (Henry et al., 2020), to better regulate activation statistics. In contrast, normalization-free designs like DyT (Zhu et al., 2025c) attempt to remove LN via learnable saturation functions.

7. Conclusion and Limitations

In this work, we propose **SiameseNorm**, a straightforward yet effective modification to the Transformer residual architecture that unifies the optimization stability of Pre-Norm with the representational capacity of Post-Norm. By decoupling LN schemes with negligible overhead, SiameseNorm enhances performance while preserving robustness.

Despite these promising results, we acknowledge two primary limitations in our current study. First, the performance gains on certain downstream tasks are not as pronounced as the significant reductions observed in pre-training perplexity. Second, we observe a more significant emergence of “massive activations” (Sun et al., 2024) compared to conventional baseline architectures. This indicates that there is still significant optimization space for the proposed architecture to fully unleash its potential.

We envision this approach as a solid foundation for future theoretical and empirical exploration into multi-stream paradigms and residual architecture designs.

8. Acknowledgment

We thank Zihan Qiu for outstanding insights and generous support, and Zhenda Xie for valuable guidance. We also thank Yifan Pu, Huaqing Zhang and Zichen Liang for helpful discussions, and Zeyu Liu for constructive suggestions on both the codebase and the writing.

References

Ainslie, J., Lee-Thorp, J., de Jong, M., Zemlyanskiy, Y., Lebron, F., and Sanghali, S. Gqa: Training generalized multi-query transformer models from multi-head checkpoints. In *Proceedings of the 2023 Conference on Empirical Methods in Natural Language Processing*, pp. 4895–4901, 2023.

Ba, J. L., Kiros, J. R., and Hinton, G. E. Layer normalization. *arXiv preprint arXiv:1607.06450*, 2016.

Bachlechner, T., Majumder, B. P., Mao, H., Cottrell, G., and McAuley, J. Rezero is all you need: Fast convergence at large depth. In *Uncertainty in Artificial Intelligence*, 2021.

Baykal, C., Cutler, D., Dikkala, N., Ghosh, N., Panigrahy, R., and Wang, X. Alternating updates for efficient transformers. *Advances in Neural Information Processing Systems*, 36:76718–76736, 2023.

Beltagy, I., Peters, M. E., and Cohan, A. Longformer: The long-document transformer. *arXiv preprint arXiv:2004.05150*, 2020.

Bisk, Y., Zellers, R., Gao, J., Choi, Y., et al. Piqa: Reasoning about physical commonsense in natural language. In *Proceedings of the AAAI conference on artificial intelligence*, volume 34, pp. 7432–7439, 2020.

Brown, T., Mann, B., Ryder, N., Subbiah, M., Kaplan, J. D., Dhariwal, P., Neelakantan, A., Shyam, P., Sastry, G., Askell, A., et al. Language models are few-shot learners. *Advances in neural information processing systems*, 33: 1877–1901, 2020.

Chen, A., Li, A., Gong, B., Jiang, B., Fei, B., Yang, B., Shan, B., Yu, C., Wang, C., Zhu, C., et al. Minimax-m1: Scaling test-time compute efficiently with lightning attention. *arXiv preprint arXiv:2506.13585*, 2025.

Child, R., Gray, S., Radford, A., and Sutskever, I. Generating long sequences with sparse transformers, 2019. URL <https://arxiv.org/abs/1904.10509>.

Choromanski, K., Likhoshesterov, V., Dohan, D., Song, X., Gane, A., Sarlos, T., Hawkins, P., Davis, J., Mohiuddin, A., Kaiser, L., et al. Rethinking attention with performers. *arXiv preprint arXiv:2009.14794*, 2020.

Clark, P., Cowhey, I., Etzioni, O., Khot, T., Sabharwal, A., Schoenick, C., and Tafjord, O. Think you have solved question answering? try arc, the ai2 reasoning challenge. *arXiv preprint arXiv:1803.05457*, 2018.

Ding, M., Yang, Z., Hong, W., Zheng, W., Zhou, C., Yin, D., Lin, J., Zou, X., Shao, Z., Yang, H., et al. Cogview: Mastering text-to-image generation via transformers. *Advances in neural information processing systems*, 34: 19822–19835, 2021.

Dosovitskiy, A. An image is worth 16x16 words: Transformers for image recognition at scale. *arXiv preprint arXiv:2010.11929*, 2020.

Geva, M., Schuster, R., Berant, J., and Levy, O. Transformer feed-forward layers are key-value memories. In *Proceedings of the 2021 Conference on Empirical Methods in Natural Language Processing*, pp. 5484–5495, 2021.

Groeneveld, D., Beltagy, I., Walsh, E., Bhagia, A., Kinney, R., Tafjord, O., Jha, A., Ivison, H., Magnusson, I., Wang, Y., et al. Olmo: Accelerating the science of language models. In *Proceedings of the 62nd annual meeting of the association for computational linguistics (volume 1: Long papers)*, pp. 15789–15809, 2024.

Gromov, A., Tirumala, K., Shapourian, H., Glorioso, P., and Roberts, D. The unreasonable ineffectiveness of the deeper layers. In *The Thirteenth International Conference on Learning Representations*, 2025.

Gu, A. and Dao, T. Mamba: Linear-time sequence modeling with selective state spaces. *arXiv preprint arXiv:2312.00752*, 2023.

Han, D., Pan, X., Han, Y., Song, S., and Huang, G. Flatten transformer: Vision transformer using focused linear attention. In *ICCV*, 2023.

Han, D., Ye, T., Han, Y., Xia, Z., Song, S., and Huang, G. Agent attention: On the integration of softmax and linear attention. In *ECCV*, 2024.

Han, D., Ye, T., Xia, Z., Chen, K., Wang, Y., Chen, H., and Huang, G. Step by step network. *arXiv preprint arXiv:2511.14329*, 2025.

He, K., Zhang, X., Ren, S., and Sun, J. Deep residual learning for image recognition. In *CVPR*, 2016.

Hendrycks, D. Gaussian error linear units (gelus). *arXiv preprint arXiv:1606.08415*, 2016.

Henry, A., Dachapally, P. R., Pawar, S. S., and Chen, Y. Query-key normalization for transformers. In *Findings of the Association for Computational Linguistics: EMNLP 2020*, pp. 4246–4253, 2020.

Huang, G., Liu, Z., Van Der Maaten, L., and Weinberger, K. Q. Densely connected convolutional networks. In *CVPR*, 2017.

Katharopoulos, A., Vyas, A., Pappas, N., and Fleuret, F. Transformers are rnns: Fast autoregressive transformers with linear attention. In *International conference on machine learning*, pp. 5156–5165. PMLR, 2020.

Kim, J., Lee, B., Park, C., Oh, Y., Kim, B., Yoo, T., Shin, S., Han, D., Shin, J., and Yoo, K. M. Peri-ln: Revisiting normalization layer in the transformer architecture. *arXiv preprint arXiv:2502.02732*, 2025.

Kitaev, N., Kaiser, Ł., and Levskaya, A. Reformer: The efficient transformer. *arXiv preprint arXiv:2001.04451*, 2020.

Li, P., Yin, L., and Liu, S. Mix-ln: Unleashing the power of deeper layers by combining pre-ln and post-ln. In *The Thirteenth International Conference on Learning Representations*, 2025.

Liu, A., Feng, B., Xue, B., Wang, B., Wu, B., Lu, C., Zhao, C., Deng, C., Zhang, C., Ruan, C., et al. Deepseek-v3 technical report. *arXiv preprint arXiv:2412.19437*, 2024.

Liu, L., Liu, X., Gao, J., Chen, W., and Han, J. Understanding the difficulty of training transformers. In *Proceedings of the 2020 Conference on Empirical Methods in Natural Language Processing (EMNLP)*, pp. 5747–5763, 2020.

Mihaylov, T., Clark, P., Khot, T., and Sabharwal, A. Can a suit of armor conduct electricity? a new dataset for open book question answering. In *Proceedings of the 2018 Conference on Empirical Methods in Natural Language Processing*, pp. 2381–2391, 2018.

Nguyen, T. Q. and Salazar, J. Transformers without tears: Improving the normalization of self-attention. In *Proceedings of the 16th International Conference on Spoken Language Translation*, 2019.

Penedo, G., Kydlíček, H., Lozhkov, A., Mitchell, M., Rafel, C. A., Von Werra, L., Wolf, T., et al. The fineweb datasets: Decanting the web for the finest text data at scale. *Advances in Neural Information Processing Systems*, 37:30811–30849, 2024.

Qiu, Z., Wang, Z., Zheng, B., Huang, Z., Wen, K., Yang, S., Men, R., Yu, L., Huang, F., Huang, S., et al. Gated attention for large language models: Non-linearity, sparsity, and attention-sink-free. *arXiv preprint arXiv:2505.06708*, 2025.

Sakaguchi, K., Bras, R. L., Bhagavatula, C., and Choi, Y. Winogrande: An adversarial winograd schema challenge at scale. *Communications of the ACM*, 64:99–106, 2021.

Shazeer, N. Glu variants improve transformer. *arXiv preprint arXiv:2002.05202*, 2020.

Srivastava, R. K., Greff, K., and Schmidhuber, J. Highway networks. *arXiv preprint arXiv:1505.00387*, 2015.

Su, J., Ahmed, M., Lu, Y., Pan, S., Bo, W., and Liu, Y. Roformer: Enhanced transformer with rotary position embedding. *Neurocomputing*, 568:127063, 2024.

Sun, M., Chen, X., Kolter, J. Z., and Liu, Z. Massive activations in large language models. In *First Conference on Language Modeling*, 2024.

Sun, W., Song, X., Li, P., Yin, L., Zheng, Y., and Liu, S. The curse of depth in large language models. *arXiv preprint arXiv:2502.05795*, 2025.

Team, K., Zhang, Y., Lin, Z., Yao, X., Hu, J., Meng, F., Liu, C., Men, X., Yang, S., Li, Z., et al. Kimi linear: An expressive, efficient attention architecture. *arXiv preprint arXiv:2510.26692*, 2025.

Touvron, H., Cord, M., Sablayrolles, A., Synnaeve, G., and Jégou, H. Going deeper with image transformers. In *ICCV*, 2021.

Touvron, H., Lavril, T., Izacard, G., Martinet, X., Lachaux, M.-A., Lacroix, T., Rozière, B., Goyal, N., Hambro, E., Azhar, F., et al. Llama: Open and efficient foundation language models. *arXiv preprint arXiv:2302.13971*, 2023a.

Touvron, H., Martin, L., Stone, K., Albert, P., Almahairi, A., Babaei, Y., Bashlykov, N., Batra, S., Bhargava, P., Bhosale, S., et al. Llama 2: Open foundation and fine-tuned chat models. *arXiv preprint arXiv:2307.09288*, 2023b.

Vaswani, A., Shazeer, N., Parmar, N., Uszkoreit, J., Jones, L., Gomez, A. N., Kaiser, Ł., and Polosukhin, I. Attention is all you need. In *NeurIPS*, 2017.

Wang, H., Ma, S., Dong, L., Huang, S., Zhang, D., and Wei, F. Deepnet: Scaling transformers to 1,000 layers. *TPAMI*, 2024.

Wang, Q., Li, B., Xiao, T., Zhu, J., Li, C., Wong, D. F., and Chao, L. S. Learning deep transformer models for machine translation. In *Proceedings of the 57th Annual Meeting of the Association for Computational Linguistics*, pp. 1810–1822, 2019.

Xie, S., Zhang, H., Guo, J., Tan, X., Bian, J., Awadalla, H. H., Menezes, A., Qin, T., and Yan, R. Residual: Transformer with dual residual connections. *arXiv preprint arXiv:2304.14802*, 2023.

Xie, Z., Wei, Y., Cao, H., Zhao, C., Deng, C., Li, J., Dai, D., Gao, H., Chang, J., Zhao, L., et al. mhc: Manifold-constrained hyper-connections. *arXiv preprint arXiv:2512.24880*, 2025.

Xiong, R., Yang, Y., He, D., Zheng, K., Zheng, S., Xing, C., Zhang, H., Lan, Y., Wang, L., and Liu, T. On layer normalization in the transformer architecture. In *International conference on machine learning*, pp. 10524–10533. PMLR, 2020.

Yang, A., Li, A., Yang, B., Zhang, B., Hui, B., Zheng, B., Yu, B., Gao, C., Huang, C., Lv, C., et al. Qwen3 technical report. *arXiv preprint arXiv:2505.09388*, 2025.

Yuan, J., Gao, H., Dai, D., Luo, J., Zhao, L., Zhang, Z., Xie, Z., Wei, Y., Wang, L., Xiao, Z., et al. Native sparse attention: Hardware-aligned and natively trainable sparse attention. In *Proceedings of the 63rd Annual Meeting of the Association for Computational Linguistics (Volume 1: Long Papers)*, pp. 23078–23097, 2025.

Zellers, R., Holtzman, A., Bisk, Y., Farhadi, A., and Choi, Y. Hellaswag: Can a machine really finish your sentence? In *Proceedings of the 57th Annual Meeting of the Association for Computational Linguistics*, pp. 4791–4800, 2019.

Zhang, B. and Sennrich, R. Root mean square layer normalization. *Advances in neural information processing systems*, 32, 2019.

Zhu, D., Huang, H., Huang, Z., Zeng, Y., Mao, Y., Wu, B., Min, Q., and Zhou, X. Hyper-connections. In *The Thirteenth International Conference on Learning Representations*, 2025a.

Zhu, D., Huang, H., Zhou, J., Huang, Z., Zeng, Y., Wu, B., Min, Q., and Zhou, X. Frac-connections: Fractional extension of hyper-connections. *arXiv preprint arXiv:2503.14125*, 2025b.

Zhu, J., Chen, X., He, K., LeCun, Y., and Liu, Z. Transformers without normalization. In *Proceedings of the Computer Vision and Pattern Recognition Conference*, pp. 14901–14911, 2025c.

Zhuo, Z., Zeng, Y., Wang, Y., Zhang, S., Yang, J., Li, X., Zhou, X., and Ma, J. Hybridnorm: Towards stable and efficient transformer training via hybrid normalization. *arXiv preprint arXiv:2503.04598*, 2025.

A. Appendix

A.1. Comparison with Existing Multi-path Designs

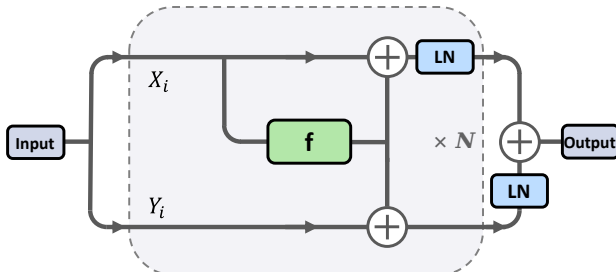


Figure 7 | Architecture of Residual (Xie et al., 2023).

ResiDual (Xie et al., 2023) The work most structurally similar to ours is ResiDual (Xie et al., 2023), as illustrated in Fig. 7. However, a fundamental difference lies in the topology: in ResiDual, the Pre-Norm stream (Y-stream) is not connected to the input of the residual block. This implies that the Y-stream acts as a global shortcut that aggregates the output of each residual block directly toward the final output, rather than an active participant in the iterative transformation process. Following the derivation in Equation (8), ResiDual’s Jacobian transition matrix is given by:

$$\frac{\partial S_{j+1}}{\partial S_j} = \begin{bmatrix} J_{LN_j^X} (I + J_{F_j}) & \mathbf{0} \\ J_{F_j} & I \end{bmatrix},$$

where $\mathbf{0}$ denotes an all-zero matrix. This implies that the Pre-Norm stream does not receive gradients related to the subsequent residual transformation F . Consequently, while the gradients remain relatively stable, they are uninformative. This structural limitation leads to the phenomenon observed in Figure 4: although the model rarely diverges completely, it frequently suffers from severe loss spikes.

Hyper-Connections (Zhu et al., 2025a) Recently, Hyper-Connections and its variant, mHC (Xie et al., 2025), have garnered significant attention within the research community. Similar to our approach, Hyper-Connections attempts to reconcile the Pre-Norm and Post-Norm paradigms. However, as noted in the mHC study, Hyper-Connections encounters training instability. To mitigate this, mHC adopts a design that more closely aligns with the Pre-Norm paradigm. Our empirical evaluations further demonstrate that SiameseNorm exhibits superior training robustness compared to Hyper-Connections. Furthermore, the Hyper-Connections framework is fundamentally compatible with our proposed method. Ablation studies in mHC indicate that H_{res} , which facilitates information mixing between parallel streams, is critical for performance gains. In contrast, SiameseNorm omits this design to maintain architectural simplicity. We

anticipate that future research will provide a unified perspective on these multi-path paradigms.

A.2. Detailed Experimental Settings

The fixed configurations for our experiments are summarized in Table 4. It should be noted that the learning rate and the total number of training tokens vary across our different experimental setups.

Table 4 | Detailed Experimental Settings for OLMo-1.3B

Category	Configuration / Value
Model architecture	
Number of Layers	16
Hidden Size	2048
Attention Heads	16
Key-Value heads	16
FFN Intermediate Size	8192
Activation Function	SwiGLU
Tied word embeddings	False
Position Embedding	RoPE
Layer Norm Type	RMSNorm, $\epsilon = 1e - 5$
Vocabulary Size	50,280
Bias Terms	None
QK-Norm	True
Initialization	Mitchell (Truncated Normal)
Training setup	
Global Batch Size	512
Max Sequence Length	2048
Optimization	
Optimizer	AdamW ($\beta_1 = 0.9, \beta_2 = 0.95$)
Weight Decay	0.1
LR Scheduler	Cosine with 2,000 warmup steps
Final LR Factor	0.1
Precision	AMP (BF16)
Gradient Clipping	1.0
Tokenizer	allenai/OLMo-1B

A.3. Training Loss and Downstream Accuracy Curves

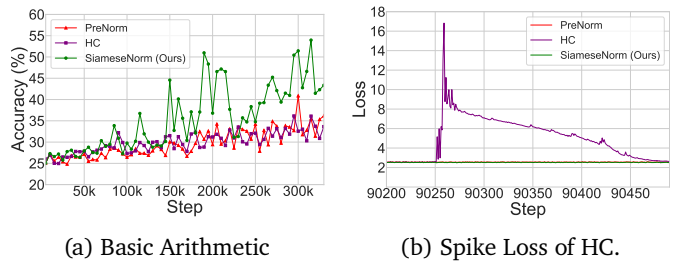


Figure 8 | Comparison of Pre-Norm (red), HC (purple) and SiameseNorm (green) on pre-training and downstream task using 350B training tokens and 2e-3 learning rate.